fMRI activation detection in wavelet signal subspace

Hamid Soltanian-Zadeh,[*1,2] Gholam-Ali Hossein-Zadeh,[1,3] Babak A. Ardekani[3]
[1]Electrical and Computer Engineering Department, University of Tehran, Tehran 14399, Iran
[2]Radiology Department, Henry Ford Hospital, Detroit, MI 48202, USA
[3]Nathan S. Kline Institute for Psychiatric Research, Orangeburg, NY 10962, USA

ABSTRACT

A new method is proposed for activation detection in event-related functional magnetic resonance imaging (fMRI). The method is based on nonparametric analysis of selected resolution levels (a subspace) in translation invariant wavelet transform (TIWT) domain. Using *a priori* knowledge about the activation signal and trends, we analyze their power in different resolution levels in TIWT domain and select an optimal set of resolution levels. A nonparametric randomization method is then applied in the wavelet domain for activation detection. This approach suppresses the effects of trends and enhances the detection sensitivity. In addition, since TIWT is insensitive to signal translations, the power analysis is robust with respect to signal shifts. Nonparametric randomization alleviates the need for assumptions about fMRI noise. The method has been applied to simulated and experimental fMRI datasets. Comparisons have been made between the results of the proposed method, a similar method in the time domain, and the cross-correlation method. The proposed method has shown superior sensitivity compared to the other methods.

Keywords: medical imaging; image processing; wavelet transform; functional magnetic resonance imaging (fMRI); activation detection; randomization.

1. INTRODUCTION

Functional magnetic resonance imaging (fMRI) is a non-invasive technique for investigating the functional anatomy of the human brain using fast MRI data acquisition methods. It relies on the sensitivity of the transverse magnetization decay rate to the variation of certain physiological parameters such as cerebral blood flow (CBF) and blood oxygenation level. Neural activity is generally accompanied by an increase in the local CBF in the activated brain areas. This causes an increase in the T_2^* decay rate and, therefore, a corresponding increase in the intensity of T_2^*-weighted MRI. By rapidly acquiring a series of MR images with pulse sequences that are sensitive to T_2^*, variations of the blood oxygenation level can be measured.[1] The fMRI measurements are physiologically filtered versions of the actual neural activity, disturbed by electronic noise and other physical and physiological artifacts.

Although blood oxygenation level dependent (BOLD) fMRI has considerable advantages over other functional imaging modalities such as EEG, MEG, and PET, its signal is limited. On a 1.5T scanner, the BOLD signal change due the experimental stimulation of the brain is approximately 1-1.5%. In addition, various sources of noise and artifacts such as subject motion, scanner calibration drifts, physiological processes such as vascular flow, heart rate, vessel motion, learning and fatigue significantly confound the fMRI signal. Therefore, the analysis method should be insensitive to these interfering signals so that activations can be accurately detected.

A variety of analysis methods have been developed for detecting brain activations in fMRI. Principal component analysis (PCA),[2] independent component analysis (ICA),[3] and fuzzy C-Means clustering,[4] are examples of model-free and nonparametric data driven methods for analyzing the fMRI data. They do not need any prior knowledge about the experiment or the hemodynamic behavior. Based on these methods, the data are classified into different groups. Usually, the contents of one class are interpreted as activation, but how the activation signal is divided between classes or eigen components is difficult to ascertain. Some of the classes separated by these methods have physiological interpretation[5-6] but most of them do not. In contrast with PCA, ICA, or clustering, model-based fMRI signal analysis methods (e.g., the general linear model[7] or the method introduced by Bullmore *et al.*[8]) assume a specific model for the fMRI signal with a specified noise structure.

* Correspondence: hamids@rad.hfh.edu

However, the structure of noise in fMRI is not well understood and remains a contentious subject.[9] The validity of the statistical models depends on the extent to which the data satisfies the underlying assumptions.

We have developed a new method for fMRI analysis using translation invariant wavelet transform (TIWT) in order to define a feature space for representing the fMRI time-series. Using prior knowledge of the activation signal and trends and by a power analysis in the TIWT domain, an optimal subspace is selected in this feature space. Then, nonparametric randomization based statistical analysis methods are applied in the selected subspace in order to identify the brain areas with significant activations. This method makes no assumptions about the noise structure or distribution.

Wavelet transforms have been previously used in fMRI signal analysis[10-11] and also in the analysis of PET images.[12] Ruttimann, *et al.*[10] applied two-dimensional (2D) wavelet transform on a difference image formed by subtracting the average "off" images from the average "on" images. Their method does not require image smoothing, takes advantage of efficient thresholding in the wavelet domain rather than the spatial domain, and decreases the number of statistical tests needed. The major limitation of their method is that much of the temporal information is lost as a result of averaging. Although there is some spatial correlation in fMRI datasets, the temporal information is more important than the spatial information. The assumption of i.i.d. noise structure is another limitation of this method. Laconte *et al.*[11] applied Wiener filtering in the wavelet domain for fMRI noise suppression. Others, e.g., references[13-15] also used wavelet transform for suppressing fMRI noise and improving detection sensitivity.

In contrast with the previous works, we use the wavelet domain coefficients directly in order to detect activation, i.e., the features extracted by wavelet transform are used directly for activation detection. A power analysis is applied in the wavelet domain in order to separate the nuisance components and to select the proper subspace. It should be noted that the idea of searching for activation in a subspace has been previously applied to fMRI data analysis by other groups. For example, in references[8,16] a subspace in the time domain was used for activation detection. Randomization analysis has also been employed in previous works for obtaining empirical distributions of fMRI statistics.[8,17] The novelty of our approach to randomization analysis is its conformity with the data exchangeability concept, which should be considered carefully in randomization studies.

2. PROPOSED ANALYSIS METHOD

Existence of significant noise and artifacts in the fMRI signal complicates the problem of activation detection in the time domain. We propose a multi-resolution decomposition of the signal to find a subspace that contains the activation components. Although random noise spreads in all sections of the wavelet transform domain almost equally, low frequency and smooth trends concentrate in the lower resolution levels. In the proposed approach, the resolution levels in which the relative power of the reference signal is greater than that of the trends are selected for analysis. Then, a nonparametric randomization based statistical analysis method is used for activation detection in the selected levels. The proposed method includes the following steps.

Step 1: Select an optimal subspace in the TIWT domain[18-20] for maximum separation between the activation and the trend components.

Step 2: Transform the fMRI data into the wavelet domain by applying TIWT on the time-series of each voxel.

Step 3: Generate a statistical parameter map by using the selected levels of resolution and compute the empirical distribution of the statistical parameter under the null hypothesis using the randomization approach.

Step 4: Using the empirical distribution obtained in Step 3, test the brain voxels for presence of activation.

The above steps are described in detail in the following sections.

2.1 Selecting wavelet basis functions and subspace

In this step, *a priori* knowledge about the trends in the fMRI signal and the neural activity are used to select the most appropriate wavelet basis and the most appropriate resolution levels (subspace) in the TIWT domain. In the selected resolution levels, the relative power of the reference signal should be greater than the relative power of trends. This ensures that any component of neural activity in the time-series will remain in these resolution levels. Unselected channels mainly contain noise and other nuisance components.

The reference signal is the expected neural system response. The most common approach for modeling the hemodynamic system is by using a linear time-invariant system,[16,21] although nonlinearity of the hemodynamic

system has also been reported.[22] Without loss of generality, we can assume that the system is linear and time-invariant. A nonlinear model can alternatively generate the reference signal if such a model is assumed. For the linear system, we assumed a gamma function[23] for the impulse response. The gamma function has two parameters and models the delay and the shape of the hemodynamic response closely. We use this function, given in (1), as the impulse response of the hemodynamic system.

$$h(t;\tau,\delta)=\begin{cases} e^{-t/\sqrt{\delta\tau}}\left(\frac{e\,t}{\tau}\right)^{\sqrt{\tau/\delta}}, & t>0 \\ 0, & t<0 \end{cases} \tag{1}$$

Using the above model, the reference signal is found by convolving the stimulation pattern (input) with the impulse response. The samples of the reference function are placed in a vector R of length N, where N is the number of time points in the fMRI experiment:

$$R=[R(0)\ R(1),\ldots,\ R(N-1)]^T \tag{2}$$

A group of nuisance components in fMRI time-series includes low frequency and smoothly varying signals, which can be called trends. The trends are usually modeled by low degree polynomials[24-25] or low frequency sine or cosine waves.[24] We choose L predefined signals as trends, each of them represented by an $N\times 1$ vector T^l. TIWT with J levels of resolution ($J = Log_2 N$) is then applied to the reference signal and the trends. Let the j-th level wavelet coefficients of the reference and trend signals be represented by vectors R_j and T_j^l ($j=1,2,\ldots J$), respectively.

$$R_j=[d_j^R(0),\ d_j^R(1),\ \ldots,\ d_j^R(N-1)]^T \tag{3}$$

$$T_j^l=[d_j^{T^l}(0),\ d_j^{T^l}(1),\ \ldots,\ d_j^{T^l}(N-1)]^T \tag{4}$$

According to a Lemma (not given here due to page limitation), we have:

$$\|R\|^2=\sum_{j=1}^{J}\frac{1}{2^j}\|R_j\|^2+\sum_{k=0}^{N-1}\frac{1}{2^J}\left[c_J^R(k)\right]^2 \tag{5}$$

$$\|T^l\|^2=\sum_{j=1}^{J}\frac{1}{2^j}\|T_j^l\|^2+\sum_{k=0}^{N-1}\frac{1}{2^J}\left[c_J^{T^l}(k)\right]^2 \tag{6}$$

We next define the indices q_j and p_j to represent the relative power content at resolution level j for the reference vector and the trends, respectively. They may be written as:

$$q_j=\frac{\frac{1}{2^j}\|R_j\|^2}{\|R\|^2} \tag{7}$$

$$p_j=\frac{1}{L}\sum_{l=1}^{L}\frac{\frac{1}{2^j}\|T_j^l\|^2}{\|T^l\|^2} \tag{8}$$

Note that the use of TIWT ensures that these indices are insensitive to signal translations. Signal translation in time results in a similar translation of the coefficients in each resolution level, but the total power of each level remains the same. Since the trends are smoother than the reference signal, we expect that p_j's are greater in the lower levels of resolution (higher j's), whereas, q_j's have greater values in the higher levels of resolution (smaller j's). Our objective is to select an optimal resolution level j_0 and perform the subsequent statistical analyses on the subspace defined by the set of resolution levels $j=1,2,\ldots, j_0$. For this purpose, we define j_0 to be the resolution level, which minimizes the following error function:

$$E(j)=\sum_{i=j+1}^{J}q_i+\sum_{i=1}^{j}p_i \tag{9}$$

This is similar to minimizing the total classification error in pattern classification applications.

The same strategy may be used to find the optimal wavelet basis. Since $E(j_0)$ shows the ability of a wavelet basis in separating the trends from the reference signal, the optimal basis should have the minimum $E(j_0)$. Thus, different bases may be compared by their $E(j_0)$. This method was used for selecting the TIWT basis functions.

After finding j_0, we remove the means of R_j's and normalize them, in order to generate a unit reference vector, R'_j , at each level of resolution.

$$R'_j = \frac{R_j - Mean(R_j)}{\left\| R_j - Mean(R_j) \right\|} \tag{10}$$

The q_j's as also normalized as follows:

$$q'_j = \frac{q_j}{\sum_{j=0}^{j_0} q_j} \tag{11}$$

2.2 Statistical parameters

Let X_i represent the vector of time-series measurements of a voxel i ($i=1,2,\ldots V$), where V is the number of intra-cerebral voxels being analyzed. We first remove the mean of the time-series, i.e.,

$$Y_i = X_i - Mean(X_i). \tag{12}$$

Then, we calculate the TIWT of the vector Y_i up to resolution level j_0 using the algorithm of Section 2 and put the coefficients of each level in a vector, remove their mean, and denote them by D_j^i, where:

$$D_j^i = [d_j^i(0),\ d_j^i(1),\ldots, d_j^i(N-1)]^T - Mean([d_j^i(0),\ d_j^i(1),\ldots,\ d_j^i(N-1)]^T) \tag{13}$$

Next, for each level we compute the following parameter:

$$s_j^i = \frac{< D_j^i, R'_j >}{\sqrt{< D_j^i, D_j^i > - < D_j^i, R'_j >^2}},\ (j = 1,\ldots, j_0) \tag{14}$$

We have defined the vector of TIWT coefficients of the reference signal at the resolution level j by R_j and the corresponding coefficients of vector X_i at this level by D_j^i. Since R'_j is a unit vector, (14) measures the cotangent of the angles between R'_j and D_j^i which is proportional to the t-test statistics.

By computing s_j^i for the j_0 levels, we have j_0 indices of similarity for different levels of resolution between the reference vector and the signal at voxel i. If voxel i has significant activation, then vectors R'_j and D_j^i are similar and the angle between them is small and therefore the s_j^i's are large. Therefore, s_j^i's can be used to decide on the activation state of the voxel. Each statistic, s_j^i, can be used alone to identify an activation map for its corresponding resolution level. These maps must be combined into a single map showing the activated brain regions. One possibility is combining them using decision fusion operators, e.g., logical AND and OR, to get the final activation map. Another approach is to use data fusion in order to combine all j_0 statistics s_j^i into a summary parameter t^i. A reasonable combination method is to define t^i to be the weighted average of s_j^i with weights proportional the relative reference signal power at level j, that is, q'_j. Thus, we have:

$$t^i = \sum_{j=1}^{j_0} s_j^i . q'_j \tag{15}$$

In the following section, we present a nonparametric approach for detecting the activated voxels using this parameter.

2.3 Randomization analysis

In order to test the statistical significance of the statistic t^i at a given voxel i, we need its probability distribution under the null hypothesis, H_0, that the voxel is not activated. A common approach for getting the distribution is to develop an analytical expression for it. For this purpose, one needs to make certain assumptions about the noise structure and distribution. Therefore, validity of the results depends on the validity of these assumptions. Another approach is the randomization method in which there is no need to make any assumptions about noise structure and distribution. The empirical distribution of the parameter under study is estimated from

the data. The basic assumption of the randomization is that, under null hypothesis, the order of data can be changed. In this method, the data is scrambled and the generated realizations of the parameter of interest are used for estimating the empirical histogram of the desired parameter. The main issue in randomization is data exchangeability under null hypothesis.[26] A set of random variables is exchangeable if (and only if) the joint distribution of these variables is invariant with respect to the positions (order of placing) of them.[26] However, in the fMRI time-series there is an obvious temporal autocorrelation whose level depends on TR of the fMRI experiment. Although there are reports on using image order scrambling[17], temporal autocorrelation suggests that the fMRI data is not exchangeable especially when TR is short.

In addition to its compatibility with the data exchangeability, the proposed randomization method preserves the MRI temporal autocorrelation. It relies on the idea that, under the null hypothesis condition, the time position of the target events in the fMRI experiment is not important. Therefore, the position of the target events in the stimulus pattern can be permutated. The outcome of each permutation of the target events is a random stimulus pattern, which produces a random reference vector. Analyzing the dataset using this random reference vector generates a random *t* map. By repeating the permutation N_{perm} times, N_{perm} random *t* maps are generated. Let us denote the *i*th random *t* map by T_i and the *t* map generated by using the actual (experimental) sequence of events by *T*. Thus, the *t* values of a voxel *n* in these maps are denoted by $T_i(n)$ and $T(n)$, respectively. These maps are used for activation detection.

2.4 Activation detection

The first step in detection is doing an omnibus test for examining the existence of any activation in the whole data set.[27] This kind of test has a strong control on the overall type I error.[27] If the data passes this test successfully, we are confident that the activations detected in the next step have not been obtained entirely by chance. The second step localizes the activations within the brain.

The omnibus null hypothesis H_0^{Ω}, which states that there is no activation in the data, is tested using the method proposed in reference.[27] The maximum value of each parameter map is computed.

$$t_l^{\max} = \underset{i=1,\ldots,V}{Max}\, T_l(i) \tag{16}$$

$$t^{\max} = \underset{i=1,\ldots,V}{Max}\, T(i) \tag{17}$$

Using the empirical histogram generated from the set of $t_l^{\max}$'s an omnibus *p* value can be computed as follows:

$$p_{omnibus} = \frac{Card\left\{ t_l^{\max} \geq t^{\max} \right\}}{N_{perm}} \tag{18}$$

where "Card" denotes the cardinality of the set. A small value of $p_{omnibus}$ indicates the presence of activation somewhere in the brain.

In the second step, we use the empirical histogram generated from the random *t* maps ($M = N_{perm}*V$ realizations of *t* under null hypothesis) to compute the *p* values for the voxels. The *p* value of voxel *i* is computed as:

$$p_i = \frac{Card\{T_j(k) \geq T(i);\ j = 1,\ldots,N_{perm},\ k = 1,\ldots,V\}}{N_{perm} * V}. \tag{19}$$

For a false alarm rate of α, we reject the null hypothesis for pixels with *p* values smaller than α and mark the corresponding voxels as active.

3. SIMULATION AND EXPERIMENTAL METHODS AND RESULTS

The proposed method for activation detection has been applied to simulated and experimental fMRI datasets and its performance has been compared to those of a similar time domain method and the conventional cross-correlation method. Image acquisition and processing details are described in the following sections.

3.1 Simulated dataset

For simulating an fMRI dataset, we added activations, trends, and noise to a base image. The base image was obtained by averaging 256 images of size 64 × 64, collected by a T_2^*-weighted gradient echo single-shot echo-planar (EPI) sequence using a 1.5 T Siemens Vision MRI scanner (Siemens AG, Erlangen, Germany). The imaging parameters were TR=1648 ms, TE=45 ms, Flip Angle=90º. The pixel size was approximately 3.91 × 3.91 mm^2 and slice thickness was 6 mm with no gaps. During data collection, the subject was at rest. The base image is shown in Fig. 1.*a*.

Each simulated time-series contained 256 time points. Gaussian noise with zero mean and standard deviation 10 was added to each time-series. Trends were simulated using first and second degree polynomials ($f(t) = t$ and $f(t) = t^2$). The amplitude of trends were different for different pixels and had a normal distribution with zero mean and standard deviation 0.01 and 0.0008 for the first and second degree polynomials, respectively.

The spatial pattern of activity is shown in Fig. 1.*b*. As in reference[28] different contrast levels (1%, 2%, 3%, and 4%) in different sizes of clusters (3, 6, 8, and 12 pixels) were added to the dataset. The hemodynamic response function parameters were $\tau = 4.73$, $\sigma = 0.0639$[23] and the reference signal was computed. The input of the block diagram was a series of 17 randomly positioned impulses corresponding to our experimental fMRI data acquisition described in Section 3.4. The reference signal was the same for both simulated and experimental fMRI data.

3.2 Comparison studies

The proposed method has been compared with two other methods. The first method is similar to the current method without the application of TIWT, i.e., the analysis is done in the time domain by the same statistical procedure. This allows evaluating the effect of TIWT on detection sensitivity. The time domain method uses a similar statistical parameter given by:

$$e^i = \frac{< Y_i, R_e >}{\sqrt{< Y_i, Y_i > - < Y_i, R_e >^2}} \tag{20}$$

$$R_e = \frac{R - Mean(R)}{\left\| R - Mean(R) \right\|} \tag{21}$$

where, R_e is a unit reference vector produced by removing the mean and normalizing the vector R in (2), and Y_i is the time-series of pixel i after its mean is removed as defined in (12). The same randomization analysis explained in Section 2.3 was used to estimate the distribution of e under the null hypothesis.

The second method used for comparison is the conventional cross-correlation method.[29] The statistic for this method is computed by:

$$c^i = \frac{< Y_i, R_e >}{\sqrt{< Y_i, Y_i >}}. \tag{22}$$

To test the significance of c^i, the correlation coefficients are usually transformed using Fisher's Z transform:

$$z^i = \frac{1}{2} \ln \frac{1 + c^i}{1 - c^i} \tag{23}$$

to generate an approximately normally distributed parameter z^i (under the null hypothesis) with mean of zero and variance of 1/(N-3).[30]

3.3 Simulation results

To select the optimal basis for the TIWT, we examined the following bases: Haar wavelet with 2 coefficents; Daubechies wavelets with 4 and 6 coefficients (which have 2 and 3 vanishing moments);[31] Battle-Lemari spline wavelets with 8 and 16 coefficients (which produce an orthonormal wavelet basis); Coiflet wavelet of degree 2 (two vanishing moments in both wavelet and scaling functions) with 6 coefficients; and Coiflet wavelet of degree 3 (three vanishing moments) with 8 coefficients.[31]

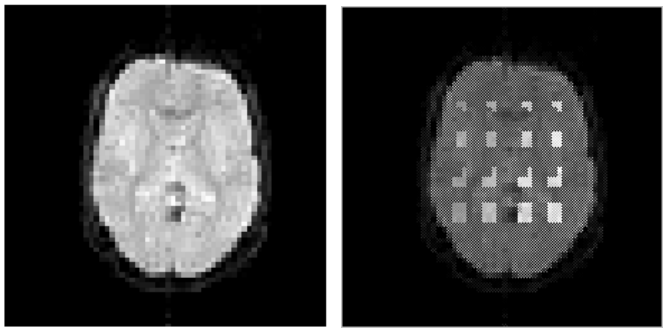

a *b*

Fig. 1. *a*) The base image used for simulation. *b*) Spatial pattern of activity. Activations were added to the dataset in the regions shown in this figure. The activation contrasts for the columns (from left to right) are 1%, 2%, 3%, and 4%, respectively.

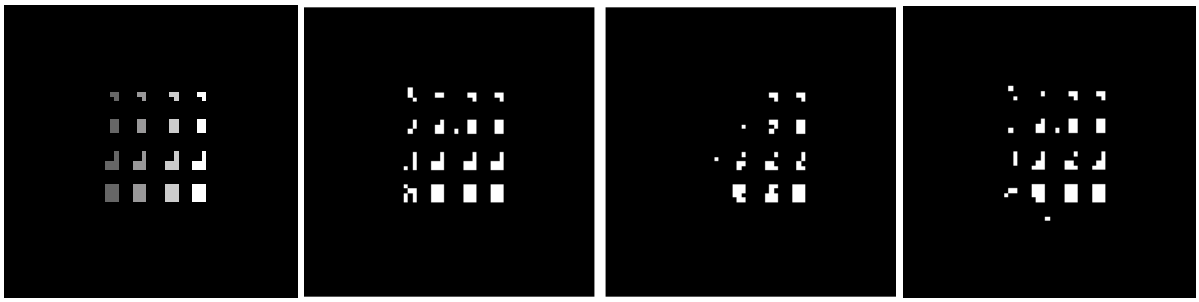

a *b* *c* *d*

Fig. 2. *a*) Actual spatial pattern of activation in simulation. *b,c,d)* Activation maps resulted form three different methods for false alarm rate of α=0.005. *b*) Proposed TIWT based method. *c*) Similar method in the time domain. *d*) Cross-correlation method.

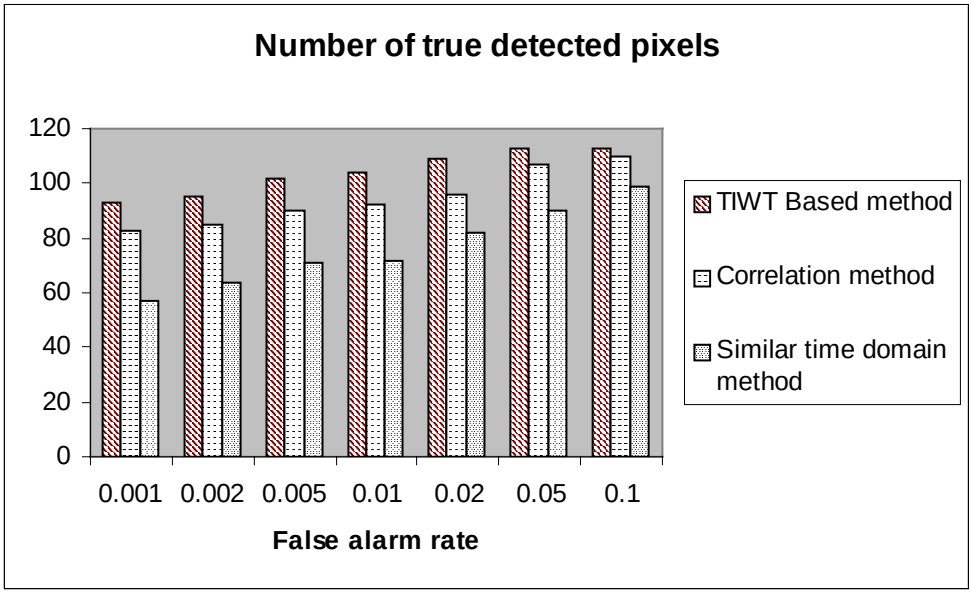

Fig. 3. Comparison of the number of correctly detected active voxels (true positives) for three different methods at different false alarm rates.

The reference signal was decomposed into $J=8$ levels of resolution. The values of the normalized power of the reference signal in each level of resolution (q_j) show that the power is mainly concentrated at higher resolution levels (lower j's). The number of trends was chosen to be $L=2$ corresponding to polynomials of degrees one and two.

After computing the p_j and q_j for different wavelet bases, the error was estimated. We found that the Battle-Lemari spline wavelet with *16* coefficients has the minimum error among all of the bases studied. Based on these results, the higher resolution levels at $j=1,2,3,4,5$, and the Battle-Lemari spline wavelet were selected as the subspace for the analysis and the basis for the TIWT, respectively.

After selecting the optimal subspace and wavelet basis, the TIWT was applied to the time-series of all voxels. The parameters s_1^i, s_2^i, s_3^i, s_4^i, s_5^i, and the final statistical parameter of the method t^i were computed for each voxel i. Randomization was performed $N_{perm}=1000$ times and random maps were generated for each of the selected levels of resolution and for the parameter t.

In the first step of detection, the omnibus test was performed for the dataset. The omnibus p value of the data set, defined by (18), was 0.001 suggesting that the dataset contains activation. In the second step, the random t maps were used for computing the empirical histogram of t under the null hypothesis.

For comparison, the randomization method was applied to the time domain method. The random maps of parameter e were computed and the omnibus test was applied, resulting in a p value of 0.001. The cross-correlation method was also applied to the simulated dataset. Fig. 2 shows the actual activation pattern along with the detected activation regions using the proposed method, the time domain approach, and the cross-correlation method for false alarm rate of $\alpha=0.005$. Note that the multi-resolution wavelet based method has detected more active pixels than the other two methods.

For comparison between sensitivities of the methods, the detection procedure was performed at different false alarm rates. Fig. 3 compares the number of correctly detected active voxels at different false alarm rates for the three methods.

3.4 fMRI experiment

The fMRI experiment was conducted using a 1.5 Tesla Siemens Vision MRI scanner (Siemens AG, Erlangen, Germany) located at the Center for Advanced Brain Imaging of the Nathan Kline Institute. Four healthy subjects were scanned. The task given to the subjects in this experiment is known as the "classic visual oddball paradigm." In this task, a train of equally spaced visual stimuli was presented to the subjects. There were two types of stimuli: the standard stimuli; and the target stimuli. The standard events occurred more frequently than the target events. The subjects were instructed to count the target stimuli silently and report the total number at the end of the experiment. The standard (frequent) visual stimulus was an image consisting of the string of white characters "OOOOO" on a dark background and occurred 93.36% of the times; the rare (target) image was the string of characters "XXXXX" and occurred 6.64% of the times. Visual stimuli were delivered to the subject via a liquid crystal display (LCD) mounted on the MRI scanner's radio frequency (RF) head coil. The LCD display was connected to the video graphics array (VGA) output of a personal computer (PC) outside the scanner room. A total of 256 images were shown to the subjects (17 targets and 239 standards) in one experimental. The inter-stimulus interval (ISI) was 1648 ms and the stimulus duration was approximately 500 ms. For the remaining time (~1148 ms) the screen was dark. The target events were distributed randomly amongst 256 trials. The subjects were given earplugs and were positioned supine and comfortably in the magnet. Cushions were placed around the subject's head in order to reduce the head motion.

Using a T_2^*-weighted gradient echo single-shot echo-planar (EPI) sequence with TR = 1648 ms, TE = 45 ms, Flip Angle = 90º, and FOV = 250×250 mm^2, a total of 256 EPI volumes were scanned from each subject. Each volume covered the entire cerebrum and the superior aspect of the cerebellum, consisting of 15 transverse slices of size 64×64 with a pixel size of approximately 3.91×3.91 mm^2 and a slice thickness of 6 mm with no gaps. The acquisition of each EPI volume was synchronized with the onset of a visual stimulus. The synchronization was achieved by triggering the MRI scanner using an external TTL pulse generated by the stimulus presentation PC. In addition to the EPI data, a high-resolution anatomical 3D T_1-weighted image volume was scanned from each subject using a magnetization-prepared rapid acquisition gradient echo (MP-RAGE) sequence. The scan parameters for this sequence were TR = 11.6 ms, TE = 4.9 ms, Flip Angle = 8º, FOV = 256×256×190 mm^3, with a matrix size of 256×256×190 voxels, yielding a 1 mm^3 isotropic voxel size.

The first four scans of functional dataset were omitted and the rest of images were registered for motion artifacts using the AFNI software package (Medical College of Wisconsin, Milwaukee, WI).[32] For separating the intra-cerebral voxels, a brain mask was generated. This mask was generated by thresholding an average image of all 252 volumes of data. Limiting the processing only to the intra-cerebral voxels resulted in a significant saving in memory and disk space. The axial MP-RAGE images were transformed into the Talairach-Tourneaux stereotactic atlas using the AFNI software package.

Since the reference signal, the homodynamic response function parameters, the trends, and the number of time points in the simulation study were chosen to be the same as this experimental dataset, the results presented in the previous section, on wavelet basis and subspace selection, were used here. In the analysis of this dataset, we also compared the proposed approach with the similar approach in time domain and the cross-correlation method. The randomization procedure was done for $N_{perm} = 500$. All subjects passed the omnibus test.

The detected activation image for each subject was resliced to 256×256×190 to match to the anatomical images. Three orthogonal slices of the results for the first subject is shown in Talairach space in Fig. 4. The bilateral activation of the supramarginal gyrus in the inferior parietal lobule (Brodmann Area 40) and the activation of the anterior cingulate are noteworthy. Both of these regions have been found activated in previous fMRI studies of the oddball task.[33-35] Fig. 5 shows the number of voxels detected by the proposed method, the time domain method, and the conventional cross-correlation method in each subject for α=0.001. Note that in all cases the proposed TIWT method outperformed the other methods.

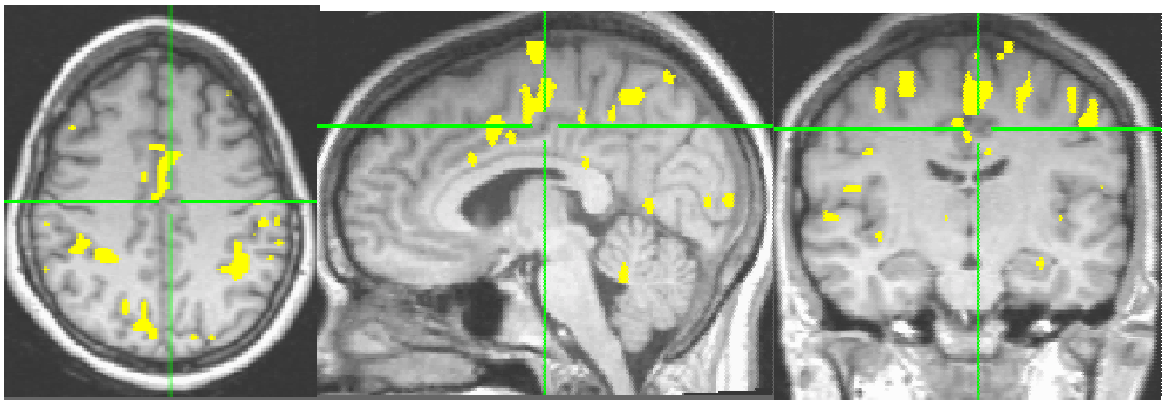

Fig. 4. Three orthogonal views of detected activation regions superimposed on the anatomical images in Talairach space for the first subject.

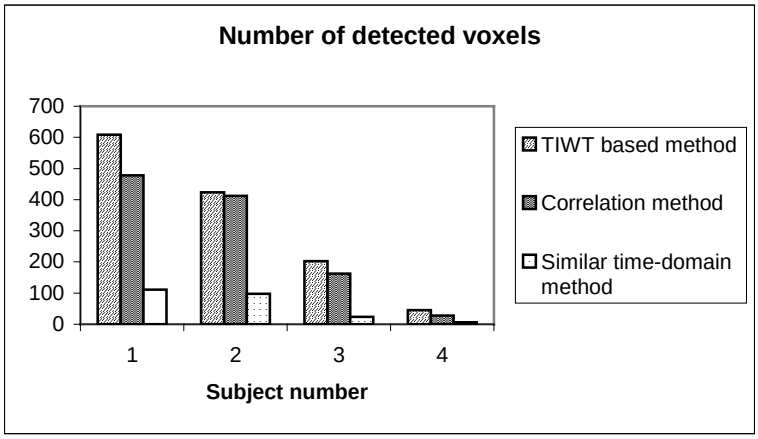

Fig. 5. Number of detected voxels in four experimental datasets using TIWT, correlation, and similar time domain methods.

4. CONCLUSION

The purpose of this paper was to present a new analysis method for fMRI with improved activation detection sensitivity. Using a simulation study, we showed that the true positive detection rate (number of correctly detected active voxels) of the proposed method is higher than those of the other two methods compared, at the same false alarm rates. The superiority of the proposed method stems from the multi-resolution decomposition of the wavelet transforms to separate the nuisance components form the fMRI signal and using proper levels of resolution. Although it is possible to have multiple detections in j_0 resolution levels, this approach not only increases the total false positives and computation, but also results in a smaller number of activations.

For the sake of completeness, we compared the proposed method to the conventional cross-correlation method as well as a similar time domain method. However, it should be noted that the comparison studies between the proposed method and the similar time domain method are most meaningful because of the algorithmic similarities and use of similar randomization analysis in these two methods. Using the randomization analysis for activation detection allows the false alarm rates of the methods to be exactly at the selected rates. Detecting more activated voxels at the same false alarm rate means superior sensitivity. In addition, these comparison studies illustrate the benefit of TIWT and conducting the detection task in the selected resolution levels of the TIWT domain.

REFERENCES

1. D. L. Bihan, *Diffusion and Perfusion Magnetic Resonance Imaging: Application to functional MRI*, Raven press, New York, 1995.
2. A. H. Andersen, D. M. Gash, and M. J. Avison, "Principal component analysis of the dynamic response measured by fMRI: A generalized linear system framework," *Magn. Reson. Imag.*, **17(6)**, pp. 795-815, 1999.
3. M. J. McKeown, S. Makeig, G. G. Brown, T.-P Jung, S. S. Kindermann, A. J. Bell, and T. J. Sejnowski, "Analysis of fMRI data by blind separation into independent spatial components," *Human Brain Mapping*, **6**, pp. 160-188, 1998.
4. M. J. Fadili, S. Ruan, D. Bloyet, and B. Mazoyer, "Unsupervised fuzzy clustering analysis of fMRI series," *proceedings of the 20th Annual International Conf. of IEEE Eng. in Med. & Biol.*, **20(2)**, pp. 696-699, 1998.
5. T. T. Liu, K. L. Miller, E. C. Wong, L. R. Frank, and R. B. Buxton, "Identifying meaningful components in independent component analysis," *NeuroImage Human Brain Mapping 2000 Meeting*, Poster No 652, 2000.
6. C. F. Beckmann, J. A. Noble, and S. M. Smith, "Artefact detection in fMRI data using independent component analysis," *NeuroImage Human Brain Mapping 2000 Meeting*, Poster No 614, 2000.
7. K. J. Friston, A. P. Holmes, K. J. Worsley, J.-P. Poline, C. D. Frith, and R. S. J. Frackowiak, "Statistical parametric maps in functional imaging: A general linear approach," *Human Brain Mapping*, **2**, pp. 189-210, 1995.
8. E. Bullmore, M. Brammer, S. C. R. Williams, S. Rabe-Hesketh, N. Janot, A. David, J. Mellers, R. Howard, and P. Sham, "Statistical methods of estimation and inference for functional MR image analysis", *Magn. Reson. Med.*, **35**, pp. 261-277, 1996.
9. E. Bullmore, C. Long, J. Suckling, J. Fadili, G. Calvert, F. Zelaya, T. A. Carpenter, and M. Brammer, "Colored noise and computational inference in neurophysiological (fMRI) time series analysis: Resampling methods in time and wavelet domains", *Human Brain Mapping*, **12**, pp. 61-78, 2001.
10. U. E. Ruttimann, M. Unser, R. R. Rawlings, D. Rio, N. F. Ramsey, V. S. Mattay, D. W. Hommer, J. A. Frank, and D. R. Weinberger, "Statistical analysis of functional MRI data in the wavelet domain," *IEEE Trans. Medical Imaging*, **17(2)**, pp. 142-154, 1998.
11. S. M. Laconte, S.-C. Ngan, and X. Hu, "Wavelet transform based wiener filtering of event-related fMRI data," *Magn. Reson. Med.*, **44**, pp. 746-757, 2000.
12. F. E. Turkheimer, M. Brett, D. Visvikis, and V. J. Cunningham, "Multiresolution analysis of emission tomography images in the wavelet domain," *Journal of Cerebral Blood Flow and Metabolism*, **19**, pp. 1189-1208, 1999.

13. J. A. Hernandez, M. Desco, A. Santos, C. S. Marta, F. D. Pozo, and P. Garcia-Barreno, "Increased sensitivity and position accuracy in the detection of brain activation by fMRI using multiscale analysis," *Computer Assisted Radiology and Surgery*, pp. 139-143, 1999.
14. A. Aldroubi and M. Unser, *Wavelets in Medicine and Biology*. Boca Raton, FL: CRC, 1996.
15. Z. Fu, Y. Hui, Z.-P. Liang, "Joint spatiotemporal statistical analysis of functional MRI data," *IEEE Conference on Image Processing ICIP*, **1**, pp.709-713, 1998.
16. B. A. Ardekani, J. Kershaw, K. Kashikura, and I. Kanno, "Activation detection in functional MRI using subspace modeling and maximum likelihood estimation," *IEEE Trans. Medical Imaging*, **18(2),** pp. 101-114, 1999.
17. M. Belmonte, and D. Yurgelun-Todd, "Permutation testing made practical for functional magnetic resonance imaging," *IEEE Trans. Medical Imaging*, **20(3)**, pp. 243-248, 2001.
18. J.-C. Pesquet, H. Krim, H. Carfantan, "Time-invariant orthonormal wavelet representation," *IEEE Trans. Signal Processing*, **44(8)**, pp. 1964-1970, 1996.
19. D. Wei, and A. C. Bovik, "Enhancement of compressed images by optimal shift invariant wavelet packet basis," *Journal of visual communication and image representaion*, **9(1)**, pp.15-24, 1998.
20. M. Unser, "Texture classification and segmentation using wavelet frames," *IEEE Trans. Image Processing*, **4(11)**, pp. 1549-1560, 1995.
21. K. J. Friston, P. Jezzard, and R. Turner, "Analysis of functional MRI time-series," *Human Brain Mapping*, **1**, pp. 153-171, 1994.
22. K. J. Friston, O. Josephs, G. Rees, R. Turner, "Nonlinear event-related response in fMRI," *Magn. Reson. Med.*, **39**, pp. 41-52, 1998.
23. K. H. Knuth, B. A. Ardekani, J. A. Helpern, "Bayesian estimation of a parameterized hemodynamic response function in an event-related fMRI experiment,", *Proc. of ISMRM*, **3**, pp. 1732, 2001.
24. R. W. Cox, "Improving the task to signal correlation in fMRI by deterending slow components," *Proc. of ISMRM*, pp. 1668, 1997.
25. M. J. Lowe, and D. P. Russell, "Treatment of baseline drifts in fMRI time series analysis," *Journal of Computer Assisted Tomography*, **23(3)**, pp. 463-473.
26. K. M. Petersson, T. E. Nichols, J.-B. Poline, and A. P. Holms, "Statistical limitations in functional neuroimaging: II signal detection and statistical inference," *Phil. Trans. Royal Society Lond. B*, **354**, pp. 1261-1281, 1999.
27. A. P. Holmes, R. C. Blair, J. D. G. Watson, and I. Ford, "Nonparametric analysis of statistic images from functional mapping experiments," *Journal of Cerebral Blood Flow and Metabolism*, **16**, pp. 7-22, 1996.
28. J. Xiong, J.-H. Gao, J. L. Lancaster, and P. T. Fox, "Assessment and optimization of functional MRI Analysis," *Human Brain Mapping*, **4**, pp. 153-167, 1996.
29. P. A. Bandettini, A. Jesmanowciz, E. C. Wong, J. S. Hyde, "Processing strategies for time-course data sets in functional MRI of the human brain," *Magn. Reson. Med.*, **30**, pp. 161-173, 1993.
30. B. A. Ardekani, and I. Kanno, "Statistical methods for detecting activated regions in functional MRI of the brain," *Magn. Reson. Imag.*, **16(10)**, pp. 1217-1225, 1998.
31. C. S. Burrus, R. A. Gopintath, and H. Guo, *Introduction to wavelets and wavelet transforms: A primer*, Prentice Hall, 1998.
32. R.W. Cox and J.S. Hyde, "Software tools for analysis and visualization of fMRI data," *NMR Biomed.*, **10**, 171-178, 1997.
33. D. E. J. Linden, D. Prvulovic, E. Formisano, M. Völlinger, F. E. Zanella, R. Goebel, and T. Dierks, "The functional neuroanatomy of target detection: an fMRI study of visual and auditory oddball tasks," *Cereb. Cortex*, **9**, pp. 815-823, 1999.
34. A. A. Stevens, P. Skudlarski, J. C. Gatenby, and J. C. Gore, "Event-related fMRI of auditory and visual oddball tasks," *Magn. Reson. Imag.*, **18**, pp. 495-502, 2000.
35. T. Yoshiura, J. Zhong, D. K. Shibata, W. E. Kwok, D. A. Shrier, and Y. Numaguchi, "Functional MRI study of auditory and visual oddball tasks," *NeuroReport*. **10**, pp. 1683-1688, 1999.